Journal of Materials Chemistry C

ROYAL SOCIETY OF CHEMISTRY

PAPER

View Article Online
View Journal | View Issue

Check for updates

Cite this: J. Mater. Chem. C, 2024, 12, 4986

$Pb_2Ga_3F_6(SeO_3)_2X_3{\cdot}2H_2O$ (X = Cl, Br): two new HTO-type members exhibiting large NLO effects mediated by ionic mixing and substitution strategies†

Lili Liu, *[a] Junbo Wang,[a] Bingchen Xiao,[a] Xunchi Li,[a] Yaoqing Chu,[a] Tongqing Sun *[b] and P. Shiv Halasyamani [c]

Received 9th February 2024,
Accepted 4th March 2024

DOI: 10.1039/d4tc00554f

rsc.li/materials-c

The anion mixing strategy and equivalent substitution of functional groups are two effective and controllable methods to improve the probability of obtaining noncentrosymmetric (NCS) structures and optimizing nonlinear optical (NLO) performance. Herein, $Pb_2Ga_3F_6(SeO_3)_2X_3{\cdot}2H_2O$ (X = Cl and Br) are discovered *via* cation group substitution and introduction of oxyfluoride [GaF_4O_2] octahedra. They are also the first examples possessing two kinds of halogen atoms in the hexagonal tungsten oxide (HTO) family. $Pb_2Ga_3F_6(SeO_3)_2Cl_3{\cdot}2H_2O$ and $Pb_2Ga_3F_6(SeO_3)_2Br_3{\cdot}2H_2O$ are isostructural and crystalize in the noncentrosymmetric trigonal space group *R*32, and they feature a three dimensional (3D) framework with HTO-type $[Ga_3F_6(SeO_3)_2]_\infty$ layers linked by $[Pb_2Br_3]_\infty$ layers. Owing to the effective arrangement of chemical functional units, $Pb_2Ga_3F_6(SeO_3)_2X_3{\cdot}2H_2O$ exhibit strong SHG responses of 4.0–4.5 × KH_2PO_4 (KDP) and short UV cut-off edges of <300 nm, which are two essential parameters for NLO practical applications. The other physical and chemical properties of title compounds were evaluated in this work using IR spectroscopy, thermal parameter measurements, and theoretical calculations.

Introduction

Through second-harmonic generation (SHG), NLO materials can achieve frequency conversion, which extends the laser output wavelength resulting in NLO crystals being indispensable in laser science.[1,2] An excellent UV NLO crystal needs to simultaneously satisfy the following attributes: (1) strong SHG intensity ($d_{ij} > 0.39$ pm V^{-1} (d_{36} KDP)), (2) short UV cutoff edge (<300 nm), (3) large optical birefringence ($\Delta n \sim 0.07$), (4) phase-matchable capability, (5) large laser damage thresholds (LDTs) (>5 GW cm^{-2}), (6) growth of large size single crystals (centimeter size), and (7) good physical–chemical stability.[3–5] The SHG coefficient is a key parameter of NLO materials that concerns their frequency doubling conversion efficiency. The general strategy to enhance the SHG coefficient is to introduce asymmetric structural units such as stereochemically active lone pair (SCALP) electrons (Pb^{2+}, Bi^{3+}, Se^{4+}, and I^{5+}),[6–12] and a distorted polyhedron constructed using d^{10} (Zn^{2+}, Cd^{2+}) or d^0 cations (Ti^{4+}, Nb^{5+}, V^{5+}, and Mo^{6+}).[13–17] However, most of these atoms undergo d–d or f–f electron transition which is heavily against the effectiveness of transparency of related materials. To enlarge the band gap, alkali and alkaline-earth metal cations without d–d or f–f electron transitions are preferred, despite these cations contributing little to enhance the SHG. Therefore, it is a challenge to achieve a balance between a large SHG effect and a wide band gap. The key to solve this problem is to select suitable fundamental building blocks (FBBs) and create a reasonable structural arrangement.

Recently, it has been shown that the anion-mixing strategy and group substitution strategy are two highly efficient synthesis strategies in the design and synthesis of new NLO materials, which have resulted in the successful syntheses of new SHG materials,[18–23] such as $CsVO_2F(IO_3)$,[24] $A_3VO(O_2)_2CO_3$ (A = K, Rb, Cs),[25] and $Pb_2TiFO(SeO_3)_2Br$.[26] The anion-mixing strategy, namely, is to introduce different kinds of anions as the ligands into one cation-centred polyhedron. The most popular anion-mixing strategy is the replacement of O^{2-} by an F^- ion to

[a] Institute of Crystal Growth, School of Materials Science and Engineering, Shanghai Institute of Technology, Shanghai 201418, China. E-mail: liulili@sit.edu.cn
[b] Key Laboratory of Weak-Light Nonlinear Photonics, Ministry of Education, School of Physics, Nankai University, Tianjin 300071, China. E-mail: suntq@nankai.edu.cn
[c] Department of Chemistry, University of Houston, 112 Fleming Building, Houston, Texas 77204, USA. E-mail: psh@uh.edu

† Electronic supplementary information (ESI) available: Crystal data, atomic coordinates, calculated dipole moments, bond lengths and angles, PXRD patterns, unit cells, cationic coordination environments, IR spectra, TG curves, and theoretical calculations. CCDC 2217261 for $Pb_2Ga_3F_6(SeO_3)_2Cl_3{\cdot}2H_2O$ and 2217262 for $Pb_2Ga_3F_6(SeO_3)_2Br_3{\cdot}2H_2O$. For ESI and crystallographic data in CIF or other electronic format see DOI: https://doi.org/10.1039/d4tc00554f

Published on 05 March 2024. Downloaded by University of Houston on 12/13/2024 5:21:31 PM.

This journal is © The Royal Society of Chemistry 2024

Published on 05 March 2024. Downloaded by University of Houston on 12/13/2024 5:21:31 PM.

construct oxyfluoride polyhedrons (for example MO_xF_y type polyhedron),[27–31] such as AB_4O_6F (A = NH_4, Na, Cs),[32,33] $K_5(NbOF_4)(NbF_7)_2$,[27] and $A_2WO_2F_3(IO_2F_2)$ (A = Rb and Cs).[34] On the one hand, O^{2-} and F^- anions have different anionic radii and electronegativities, which can break the original structure and symmetry of pure oxyanions (such as MO_x type polyhedrons) and will result in large polarizability and deformability, which can simultaneously improve the possibility of macroscopic NCS and birefringence. On the other hand, F^- can modify the electronic band structure of materials because of the lower energy of F-2p states compared with that of O-2p states, and then adjust the cutoff edge to blue-shift by replacing O^{2-} sites of oxyanions.[27,35,36] Therefore, the anion-mixing strategy between O^{2-} and F^- allows regulating the composition, symmetry, polarizability, and transmittance of materials as well as improving their comprehensive NLO performance. Group substitution is a chemical substitution-oriented design strategy, which is to directly modify the crystal structure of the known prototype compound to retain good original structural genes and improve optical properties.[24] It is well-known that HTO-type selenite and tellurite represent an important family of SHG materials, and the structural feature of this family is that d^0 TM-centred octahedral anionic layers are capped on one or both sides by $[SeO_3]^{2-}$/$[TeO_3]^{2-}$ groups.[37] Many HTO-type compounds have been reported, like $AGa_3F_6(SeO_3)_2$ (A = NH_4, K, Rb, Cs), $Cs(TiOF)_3(SeO_3)_2$, $A_2(WO_3)_3(SeO_3)$(A = NH_4, Rb, Cs), $A_2(WO_3)_3(TeO_3)$ (A = Rb, Cs), and $A_2(MoO_3)_3(SeO_3)_2$ (A = Rb, Cs, Tl, NH_4).[37–41] However, most HTO-type materials exhibit non-phase matchability, which can be attributed to their intrinsically small birefringence. To improve the non-phase matchability problem of HTO-materials, in the study of Prof. Chi Zhang, $[GaO_2F_4]^{5-}$ units coming from main group were introduced to replace d^0 TM-O_6 units based on known $A(VO_2)_3(SeO_3)_2$ (A = Rb, Cs) through group substitution and anion-mixing strategies, and then compounds $AGa_3F_6(SeO_3)_2$ (A = Rb, Cs) were obtained that exhibit strong phase-matchable SHG responses (5.0–6.0 × KDP at 1064 nm).[37]

Inspired by the above ideas, two new NCS selenites, $Pb_2Ga_3F_6(SeO_3)_2X_3{\cdot}2H_2O$ (X = Cl and Br), were discovered by our group based on group substitution and anion-mixing strategies. $Pb_2Ga_3F_6(SeO_3)_2X_3{\cdot}2H_2O$ feature HTO-type $[Ga_3F_6(SeO_3)_2]_\infty$ layers and have large SHG intensities (4.0–4.5 × KDP at 1064 nm) and wide band gaps (4.59 and 4.13 eV). After studying the structures and properties of HTO-type selenites reported in the ICSD database (see Table S1, ESI†), it is worth noting that $Pb_2Ga_3F_6(SeO_3)_2X_3{\cdot}2H_2O$ (X = Cl and Br) are the first two compounds including two different halogen atoms and exhibit a better balance between a large SHG effect and wide band gap in the current HTO-type selenite family.

Experimental

Caution: *Hydrofluoric acid is toxic and corrosive! It must be handled with extreme caution and appropriate protective equipment and training.*

Reagents

$PbCl_2$ (Alfa Aesar, 98%), $PbBr_2$ (Alfa Aesar, 98%), Ga_2O_3 (Alfa Aesar, 99.99%), SeO_2 (Alfa Aesar, 99.4%) and HF (Alfa Aesar, 48–51%) were used as received.

Syntheses

All the reported compounds were prepared by hydrothermal methods. The loaded compositions are $PbCl_2$ (0.28 g), Ga_2O_3 (0.14 g), SeO_2 (0.11 g), HF (~0.05 mL) and H_2O (5 mL) for $Pb_2Ga_3F_6(SeO_3)_2Cl_3{\cdot}2H_2O$, and $PbBr_2$ (0.37 g), Ga_2O_3 (0.14 g), SeO_2 (0.11 g), HF (~0.05 mL) and H_2O (5 mL) for $Pb_2Ga_3F_6(SeO_3)_2Br_3{\cdot}2H_2O$. The reactions were carried out at 230 °C for 4 days, followed by slow cooling to 100 °C at a rate of 2 °C h^{-1}. And, then the temperature was cooled to room temperature for 5 hours. The final pH value of the reaction media was close to 1. Finally, the products were ultrasonically washed with deionized water, and many colourless thin plate-shaped crystals were obtained with yields of ~65% and ~50% based on $PbBr_2$ for $Pb_2Ga_3F_6(SeO_3)_2Cl_3{\cdot}2H_2O$ and $Pb_2Ga_3F_6(SeO_3)_2Br_3{\cdot}2H_2O$, respectively. The purities of samples were confirmed by X-ray diffraction (XRD) studies (Fig. S1, ESI†).

Powder X-ray diffraction

Powder XRD measurements were carried out at room temperature using a PANalytical X'Pert PRO diffractometer equipped with Cu Kα radiation (λ = 1.5418 Å). Data were collected in the two-theta range of 10–70° with a step scan width of 0.008° and a scan time of 0.5 s. The powder XRD patterns for the powder samples of $Pb_2Ga_3F_6(SeO_3)_2Cl_3{\cdot}2H_2O$ and $Pb_2Ga_3F_6(SeO_3)_2Br_3{\cdot}2H_2O$ are shown in Fig. S1 (ESI†). As seen in Fig. S1 (ESI†), the experimental and calculated diffraction patterns are in good agreement.

Structural characterization

The crystal structures of $Pb_2Ga_3F_6(SeO_3)_2Cl_3{\cdot}2H_2O$ and $Pb_2Ga_3F_6(SeO_3)_2Br_3{\cdot}2H_2O$ were determined by single crystal X-ray diffraction. Data were collected on a Bruker SMART APEX2 diffractometer equipped with a 4K CCD area detector using graphite-monochromated Mo Kα radiation (λ = 0.71073 Å) and were integrated with the SAINT program.[42] A multi-scan technique was applied for the absorption corrections. The structures were solved by direct methods using SHELXS-97.[43,44] All atoms in the structure were refined using full matrix least-squares techniques, and final least-squares refinement was on F_o^2 with data having $F_o^2 \geq 2\sigma(F_o^2)$. All two structures were checked for possible missing symmetry with PLATON, and no higher symmetry was found.[45] The Flack parameters were refined to 0.032(18) and 0.002(11) for $Pb_2Ga_3F_6(SeO_3)_2Cl_3{\cdot}2H_2O$ and $Pb_2Ga_3F_6(SeO_3)_2Br_3{\cdot}2H_2O$, respectively, which confirm the correctness of their absolute structures. Crystal data and structure refinement information for the two compounds are listed in Table 1. The final refined atomic positions, isotropic thermal parameters, and bond valence sum (BVS) calculations[46] are given in Table S2 (ESI†), and selected bond lengths and angles are listed in Table S3 (ESI†).

Published on 05 March 2024. Downloaded by University of Houston on 12/13/2024 5:21:31 PM.

Table 1 Crystal data and structure refinement for $Pb_2Ga_3F_6(SeO_3)_2Cl_3{\cdot}2H_2O$ and $Pb_2Ga_3F_6(SeO_3)_2Br_3{\cdot}2H_2O$

Formula	$Pb_2Ga_3F_6(SeO_3)_2Cl_3{\cdot}2H_2O$	$Pb_2Ga_3F_6(SeO_3)_2Br_3{\cdot}2H_2O$
F_w	1133.84	1267.22
Space group	Trigonal, *R*32	
a (Å)	7.2103(5)	7.2307(8)
c (Å)	28.232(3)	29.057(3)
Volume (Å^3)	1271.1(2)	1315.6(3)
Z	3	3
D_{calcd} (Mg m^{-3})	4.444	4.798
μ (mm^{-1})	29.366	34.749
GOF on F^2	1.125	1.018
R/wR [$I > 2\sigma(I)$][a]	0.0310/0.0772	0.0201/0.0446
R/wR (all data)[a]	0.0313/0.0775	0.0207/0.0448
Flack parameter	0.024(16)	0.003(11)

[a] $R_1 = \Sigma||F_o| - |F_c||/\Sigma|F_o|$ and $wR_2 = [\Sigma w(F_o^2 - F_c^2)^2/\Sigma wF_o^4]^{1/2}$ for $F_o^2 > 2\sigma(F_o^2)$.

Infrared spectroscopy

The infrared spectra (IR) of $Pb_2Ga_3F_6(SeO_3)_2Cl_3{\cdot}2H_2O$ and $Pb_2Ga_3F_6(SeO_3)_2Br_3{\cdot}2H_2O$ in the 500–4000 cm^{-1} range were recorded by using a Thermo Scientific Nicolet iS10 FT-IR Spectrometer at room temperature.

UV-vis-NIR diffuse reflectance spectroscopy

The UV-vis-NIR diffuse reflectance spectra of $Pb_2Ga_3F_6(SeO_3)_2Cl_3{\cdot}2H_2O$ and $Pb_2Ga_3F_6(SeO_3)_2Br_3{\cdot}2H_2O$ were measured at room temperature with a Cary 5000 UV-vis-NIR spectrophotometer in the 200–1000 nm wavelength range.

Thermal analysis

The thermal properties were carried out on an EXSTAR TG/DTA 6300 in the temperature range from room temperature to 600 °C with a heating and cooling rate of 10 °C min^{-1} in flowing N_2.

SHG measurements

Powder SHG was measured by using the Kurtz–Perry method at 1064 nm.[47] Polycrystalline $Pb_2Ga_3F_6(SeO_3)_2Cl_3{\cdot}2H_2O$ and $Pb_2Ga_3F_6(SeO_3)_2Br_3{\cdot}2H_2O$ and KDP were ground and sieved into distinct particle size ranges (<20, 20–45, 45–63, 63–75, 75–90, and 90–125 μm). Sieved KDP powder was used as the reference. The samples were placed in 1 mm thick fused silica tubes. The intensity of the frequency doubled radiation from the samples was measured using a photomultiplier tube.

Theoretical calculations

The CASTEP package was employed to perform self-consistent field (SCF) and geometry optimization (GO) calculations by using Broyden–Fletcher–Goldfarb–Shanno methods, with the norm-conserving pseudopotentials (NCPs).[48] The exchange–correlation functional was the Perdew–Burke–Ernzerhof (PBE) functional within the generalized gradient approximation (GGA).[49,50] The plane-wave energy cutoff was set as 940 eV. The adopted convergence tolerance energy and self-consistent field tolerance were 5×10^{-6} eV per atom and 10^{-6} eV per atom, respectively. The *k*-point separation for each material is set as $4 \times 4 \times 2$ in the Brillouin zone for the SCF. After optimization, the optics calculation will be performed subsequently. The linear optical properties were examined based on the dielectric function $\varepsilon(\omega) = \varepsilon_1(\omega) + i\varepsilon_2(\omega)$. The imaginary part of a dielectric function ε_2 can be calculated based on the electronic structures and the real part is obtained using Kramers–Kronig transformation; accordingly, the refractive indices and the birefringence (Δn) can be calculated.

Results and discussion

Crystal structure

Single-crystal XRD analyses revealed that $Pb_2Ga_3F_6(SeO_3)_2Br_3{\cdot}2H_2O$ and $Pb_2Ga_3F_6(SeO_3)_2Cl_3{\cdot}2H_2O$ are isostructural, both crystallizing in the nonpolar NCS space group *R*32 (No. 155). Accordingly, only a representative structure, $Pb_2Ga_3F_6(SeO_3)_2Br_3{\cdot}2H_2O$, will be discussed in detail. Fig. S2 (ESI†) shows the structure of $Pb_2Ga_3F_6(SeO_3)_2Br_3{\cdot}2H_2O$. In its asymmetric cell, there is one crystallographically independent Pb atom, one Ga atom, one Se atom, one Br atom, one F atom, two O atoms, and two H atoms. As shown in Fig. 1a, $Pb_2Ga_3F_6(SeO_3)_2Br_3{\cdot}2H_2O$ features a 3D framework, composed of $[Ga_3F_6(SeO_3)_2]_\infty^-$ anionic layers and $[Pb_2Br_3]_\infty^+$ cationic layers. In the structure, the Ga atom is surrounded by two apical O atoms and four equatorial F atoms to form the $[GaF_4O_2]$ group, which extend on the *ab* plane to build the $[Ga_3F_6O_6]_\infty$ layer through sharing

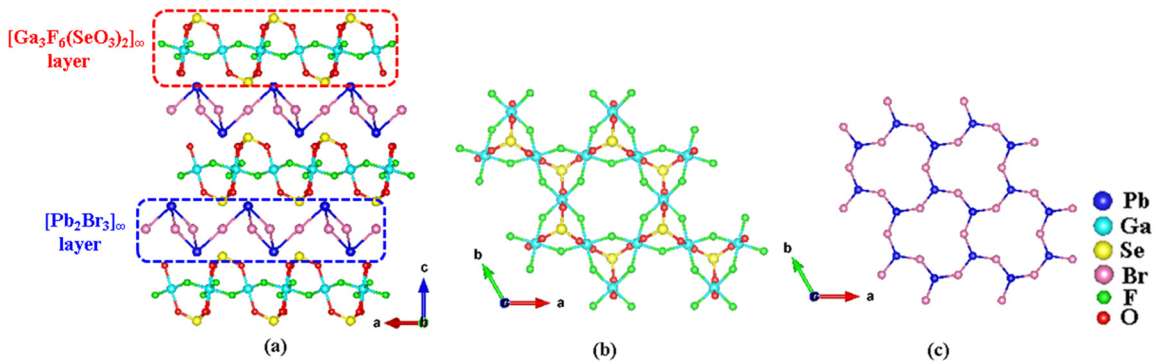

Fig. 1 Crystal structure of $Pb_2Ga_3F_6(SeO_3)_2Br_3{\cdot}2H_2O$. (a) Crystal structure of $Pb_2Ga_3F_6(SeO_3)_2Br_3{\cdot}2H_2O$ seen along the *b*-axis. (b) $[Ga_3F_6(SeO_3)_2]_\infty$ layer. (c) $[Pb_2Br_3]_\infty$ layer seen along the *b*-axis. Pb–O bonds were omitted for clarity.

 This journal is © The Royal Society of Chemistry 2024

Published on 05 March 2024. Downloaded by University of Houston on 12/13/2024 5:21:31 PM.

common F atoms. And then, SeO_3 groups cap both sides of the $[Ga_3F_6O_6]_\infty$ layer to form the HTO-type $[Ga_3F_6(SeO_3)_2]_\infty$ layer (Fig. 1b). As shown in Fig. 1c, each Pb is bonded to three Br atoms to form the $PbBr_3$ group, and then $PbBr_3$ groups were arranged on the *ab* plane end to end to construct the $[Pb_2Br_3]_\infty$ layer. $[Ga_3F_6(SeO_3)_2]_\infty$ layers and $[Pb_2Br_3]_\infty$ layers were stacked alternately along the *c*-axis and linked together through Pb–O bonds to build the whole crystal structure of $Pb_2Ga_3F_6(SeO_3)_2Br_3{\cdot}2H_2O$.

Coordination environments of cations in $Pb_2Ga_3F_6(SeO_3)_2Br_3{\cdot}2H_2O$ are shown in Fig. S3 (ESI†). The Pb atom is coordinated with three O atoms, three F atoms and three Br atoms to form a sphere-like $[PbO_3F_3Br_3]$ polyhedron that shows weak chemical stereoscopic activity. The Se atom is bonded to three O atoms to form the SeO_3 pyramid. The Ga atom connects with two O atoms and four F atoms to form the $[GaF_4O_2]$ group. In the structure, the Pb–O bond is 2.870(4) Å, the Pb–Br bond is 2.915(6) Å, the Pb–F bond is 2.869(6) Å, the Se–O bond is 1.706(4) Å, the Ga–F bond is 1.950(7) Å and the Ga–O bond is 1.951(4) Å. The calculated bond valence sum (BVS) values of Pb, Ga, Se, Br, F, O(1) and O(2) are +2.24, +2.73, +3.99, −1.06, −0.90, −1.88 and −1.69, respectively, which are in accordance with their corresponding oxidation states of +2, +3, +4, −1 and −2 (Table S2, ESI†).

Structural evolution from $A(VO_2)_3(SeO_3)_2/AGa_3F_6(SeO_3)_2$ (A = Rb, Cs) to $Pb_2Ga_3F_6(SeO_3)_2X_3{\cdot}2H_2O$

In this part, we discuss how to obtain the title compounds $Pb_2Ga_3F_6(SeO_3)_2X_3{\cdot}2H_2O$ through remoulding known $A(VO_2)_3(SeO_3)_2/AGa_3F_6(SeO_3)_2$ (A = Rb, Cs). Here, the A atom is set as the Rb atom.

From Fig. 1 and 2, it is clear that $RbGa_3F_6(SeO_3)_2$, $Rb(VO_2)_3(SeO_3)_2$ and title $Pb_2Ga_3F_6(SeO_3)_2X_3{\cdot}2H_2O$ compounds are all sandwich-like structures, composed of alternately stacked anionic layers and cationic layers. The so-called anionic layers have similar components, and they are formed by octahedra and SeO_3 groups. As shown in Fig. 1 and 2a, $Pb_2Ga_3F_6(SeO_3)_2X_3{\cdot}2H_2O$ and $RbGa_3F_6(SeO_3)_2$ possess same anionic $[Ga_3F_6(SeO_3)_2]_\infty$ layers, in which $[GaF_4O_2]$ octahedra form the basic layer skeleton and then the SeO_3 groups are capped on it. For $Rb(VO_2)_3(SeO_3)_2$, the Ga atoms are changed as V atoms, and all the F atoms are remoulded as O atoms to maintain the charge balance, and then to form the $[V_3O_6(SeO_3)_2]_\infty$ layers (Fig. 2b). $[Ga_3F_6(SeO_3)_2]_\infty$ and $[V_3O_6(SeO_3)_2]_\infty$ layers are the typical structural character of the HTO family. After the construction of $[Ga_3F_6(SeO_3)_2]_\infty$ or $[V_3O_6(SeO_3)_2]_\infty$ anionic layers, the cationic part plugs in the space between the anionic layers. For $RbGa_3F_6(SeO_3)_2$ and $Rb(VO_2)_3(SeO_3)_2$, they have a very similar crystal structure: Rb atoms are inserted into the gaps between two adjacent $[Ga_3F_6(SeO_3)_2]_\infty$ or $[V_3O_6(SeO_3)_2]_\infty$ layers (Fig. 2). But for the title compounds $Pb_2Ga_3F_6(SeO_3)_2X_3{\cdot}2H_2O$, the cationic part is 2D $[Pb_2X_3]_\infty^+$ layers, not isolated cations. In another word, cationic $[Pb_2X_3]^+$ layers take the place of equivalent A^+ ions to achieve the structural transformation from known $RbGa_3F_6(SeO_3)_2/Rb(VO_2)_3(SeO_3)_2$ to $Pb_2Ga_3F_6(SeO_3)_2X_3{\cdot}2H_2O$.

Interlayer inclusion is the biggest difference between title $Pb_2Ga_3F_6(SeO_3)_2X_3{\cdot}2H_2O$ and $RbGa_3F_6(SeO_3)_2/Rb(VO_2)_3(SeO_3)_2$, which lead to the different layer distances. As shown in Fig. 3, the distance between $[Ga_3F_6(SeO_3)_2]_\infty$ layers in $Pb_2Ga_3F_6(SeO_3)_2X_3{\cdot}2H_2O$ is as large as 9.69 Å; the interlamellar spacing in $RbGa_3F_6(SeO_3)_2/Rb(VO_2)_3(SeO_3)_2$ is only 5.83/5.73 Å, obviously smaller than that of $Pb_2Ga_3F_6(SeO_3)_2X_3{\cdot}2H_2O$.

IR spectra

The IR spectra of $Pb_2Ga_3F_6(SeO_3)_2X_3{\cdot}2H_2O$ are shown in Fig. S4 (ESI†). It is obvious that $Pb_2Ga_3F_6(SeO_3)_2Cl_3{\cdot}2H_2O$ and $Pb_2Ga_3F_6(SeO_3)_2Br_3{\cdot}2H_2O$ exhibit almost similar IR spectra. The stretching vibration of H_2O and OH is observed at $\sim$3250 cm^{-1}. The bending vibrations of H_2O are observed at $\sim$1600 cm^{-1}. The peaks between 1000 and 700 cm^{-1} are attributed to the asymmetric stretching vibration of the SeO_3 units. The vibrational peak at 490 cm^{-1} can be assigned to coupling mode of the symmetric bridge Ga–F bond and asymmetric terminal Ga–F bond vibrations.[51–55]

UV-vis-NIR diffuse reflectance spectra

The optical diffuse reflectance spectrum measurements indicate that the absorption edges of $Pb_2Ga_3F_6(SeO_3)_2Cl_3{\cdot}2H_2O$ and $Pb_2Ga_3F_6(SeO_3)_2Br_3{\cdot}2H_2O$ are approximately 270 and 300 nm corresponding the optical band gaps of 4.59 and 4.13 eV, respectively (Fig. 4). We observe that the absorption edges show a red shift gradually from $Pb_2Ga_3F_6(SeO_3)_2Cl_3{\cdot}2H_2O$ to $Pb_2Ga_3F_6(SeO_3)_2Br_3{\cdot}2H_2O$ after the Br atom replacing the Cl atom, which is attributed to the relatively smaller electronegativity of the Br atom. Compared with the HTO-type compounds listed in Table S1 (ESI†), it is worth noting that $Pb_2Ga_3F_6(SeO_3)_2X_3{\cdot}2H_2O$ display the second broadest band gap in the current NLO HTO-type selenite family ($NH_4(GaF_2)_3(SeO_3)_2$ has the widest band gap in this family[41]).

Thermal behaviour

Results of the TG analyses demonstrate that $Pb_2Ga_3F_6(SeO_3)_2Cl_3{\cdot}2H_2O$ and $Pb_2Ga_3F_6(SeO_3)_2Br_3{\cdot}2H_2O$ undergo two steps of weight loss before 450 °C (Fig. S5, ESI†). During this process, the observed weight losses of $\sim$20% and 22% are very close to the calculated values of 21.20 and 22.76% for $Pb_2Ga_3F_6(SeO_3)_2Cl_3{\cdot}2H_2O$ and $Pb_2Ga_3F_6(SeO_3)_2Br_3{\cdot}2H_2O$, respectively: the first step corresponds to the release of H_2O molecules, and the second step corresponds to the release of SeO_2. After 450 °C, a faster weightlessness occurs in the TG curve of $Pb_2Ga_3F_6(SeO_3)_2Br_3{\cdot}2H_2O$, compared with that of $Pb_2Ga_3F_6(SeO_3)_2Cl_3{\cdot}2H_2O$. The reason may be that the release of Cl and Br dominates this stage, while the proportion of Br in $Pb_2Ga_3F_6(SeO_3)_2Br_3{\cdot}2H_2O$ is larger than the proportion of Cl in $Pb_2Ga_3F_6(SeO_3)_2Cl_3{\cdot}2H_2O$. Therefore, the rate of weight loss for $Pb_2Ga_3F_6(SeO_3)_2Br_3{\cdot}2H_2O$ is relatively faster after 450 °C.

SHG measurements

The SHG effects of $Pb_2Ga_3F_6(SeO_3)_2Cl_3{\cdot}2H_2O$ and $Pb_2Ga_3F_6(SeO_3)_2Br_3{\cdot}2H_2O$ were tested under 1064 nm irradiation since they adopt the asymmetric space group and have short

Published on 05 March 2024. Downloaded by University of Houston on 12/13/2024 5:21:31 PM.

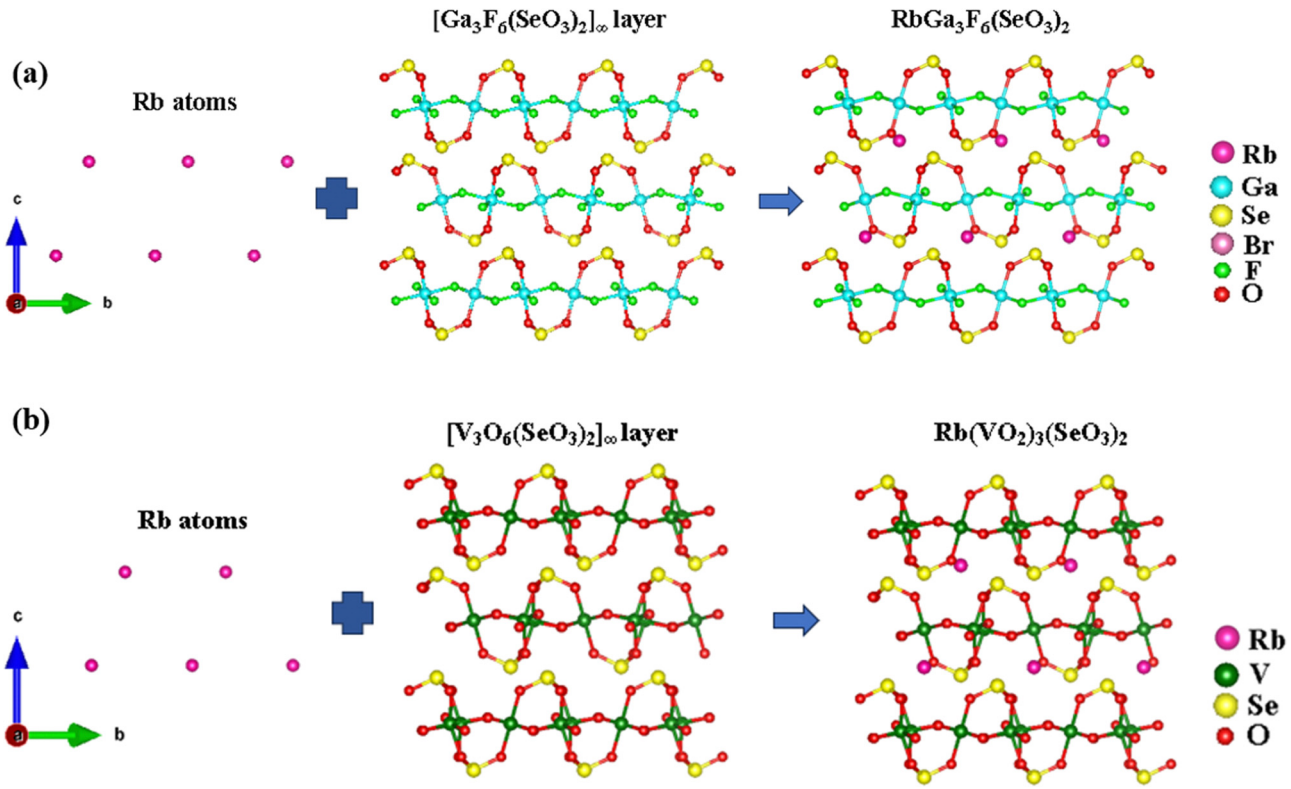

Fig. 2 Crystal structures of (a) $RbGa_3F_6(SeO_3)_2$ and (b) $Rb(VO_2)_3(SeO_3)_2$. Rb–O bonds are omitted for clarity.

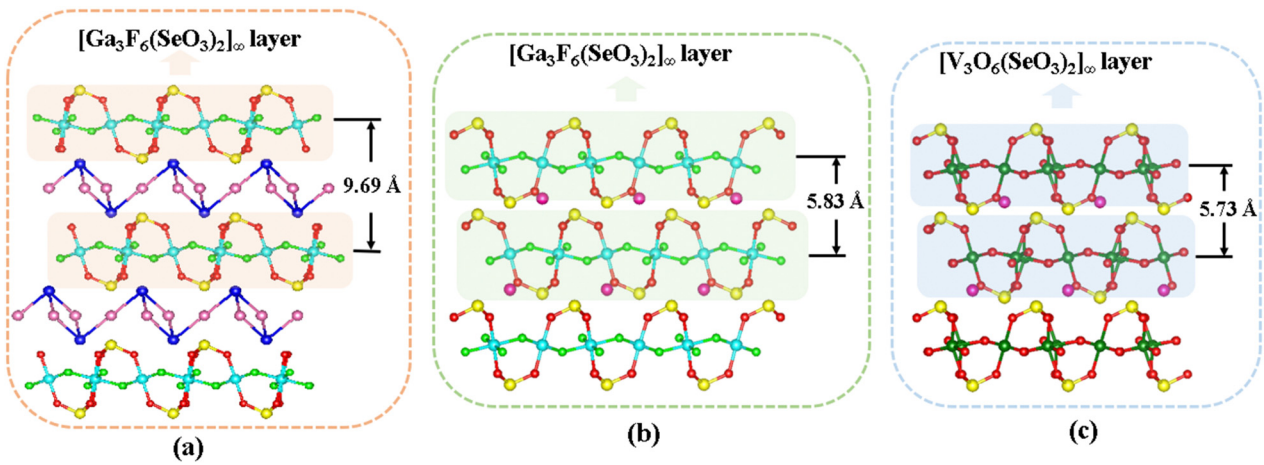

Fig. 3 Structural comparison among (a) $Pb_2Ga_3F_6(SeO_3)_2X_3{\cdot}2H_2O$, (b) $RbGa_3F_6(SeO_3)_2$ and (c) $Rb(VO_2)_3(SeO_3)_2$. H_2O molecules, Pb–O bonds and Rb–O bonds are omitted for clarity.

absorption edges. The results shown in Fig. 5 indicate that both samples cannot achieve phase matching behaviour; however, they still exhibit strong SHG effects 4.0 and 4.5 times of KDP with 63–75 μm particle size. Fig. 6 displays the band gaps and SHG effects of the current HTO-type family, in which compounds 12–15 show super SHG effects, about 7.0–12.0 × KDP, and compounds 6–11 show large SHG effects, about 4.0–6.0 × KDP. Compound 16 has the widest band gap; however, its SHG effect is only 1.1 × KDP. In summary, most of them have a relatively narrow band gap of around 3.0 eV, which limits their application wavelength and LDT. Interestingly, it is clearly demonstrated that the title compounds $Pb_2Ga_3F_6(SeO_3)_2Cl_3{\cdot}2H_2O$ and $Pb_2Ga_3F_6(SeO_3)_2Br_3{\cdot}2H_2O$ (compounds 6 and 7) have relatively wider optical band gaps in the current HTO-type family. Therefore, title compounds $Pb_2Ga_3F_6(SeO_3)_2X_3{\cdot}2H_2O$ achieve a better balance between the band gap and the SHG effect in the HTO family.

 This journal is © The Royal Society of Chemistry 2024

Published on 05 March 2024. Downloaded by University of Houston on 12/13/2024 5:21:31 PM.

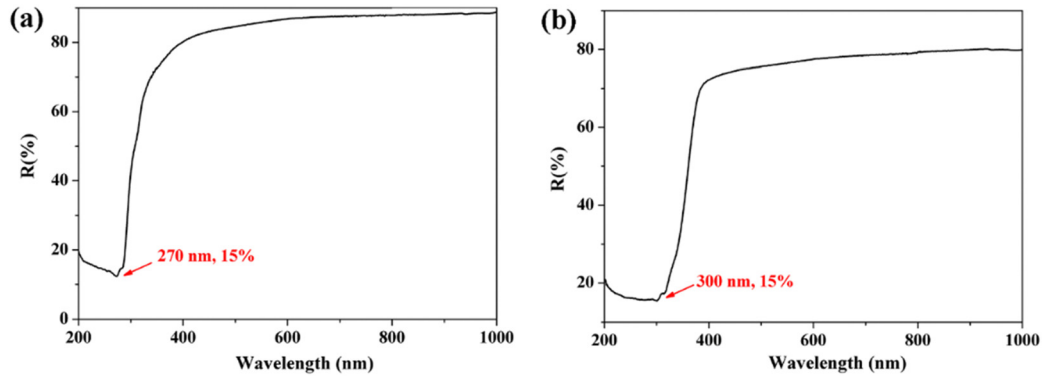

Fig. 4 The UV-vis-NIR diffuse reflectance spectra of (a) $Pb_2Ga_3F_6(SeO_3)_2Cl_3{\cdot}2H_2O$ and (b) $Pb_2Ga_3F_6(SeO_3)_2Br_3{\cdot}2H_2O$.

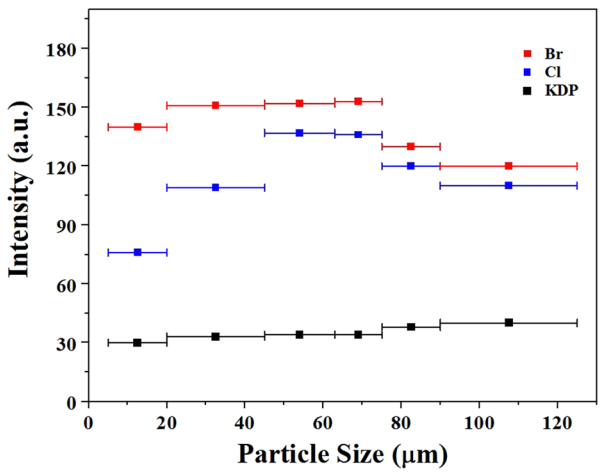

Fig. 5 SHG intensities of $Pb_2Ga_3F_6(SeO_3)_2Cl_3{\cdot}2H_2O$ and $Pb_2Ga_3F_6(SeO_3)_2Br_3{\cdot}2H_2O$.

Theoretical calculations

The calculated band gaps of $Pb_2Ga_3F_6(SeO_3)_2Cl_3{\cdot}2H_2O$ and $Pb_2Ga_3F_6(SeO_3)_2Br_3{\cdot}2H_2O$ compounds are 3.84 and 3.10 eV, respectively, which are smaller than the experimental values, as the GGA-PBE underestimates the band gap (Fig. S6, ESI†). The calculated refractive index curves of the title compounds are plotted in Fig. S7 (ESI†). The introduction of SCALP cations is an effective method,[56–59] but it illustrates that the calculated birefringences of two title compounds are about 0.02 and 0.01 at 1064 nm, which are not large enough to satisfy the condition of phase matching. So, despite that $Pb_2Ga_3F_6(SeO_3)_2Cl_3{\cdot}2H_2O$ and $Pb_2Ga_3F_6(SeO_3)_2Br_3{\cdot}2H_2O$ show large SHG effects (4.0–4.5 × KDP), they are not phase-matchable as shown in Fig. 5.

Conclusions

In summary, $Pb_2Ga_3F_6(SeO_3)_2X_3{\cdot}2H_2O$ (X = Cl, Br) compounds were obtained as two new members of the HTO family, and they are the first examples possessing two kinds of halogen atoms in

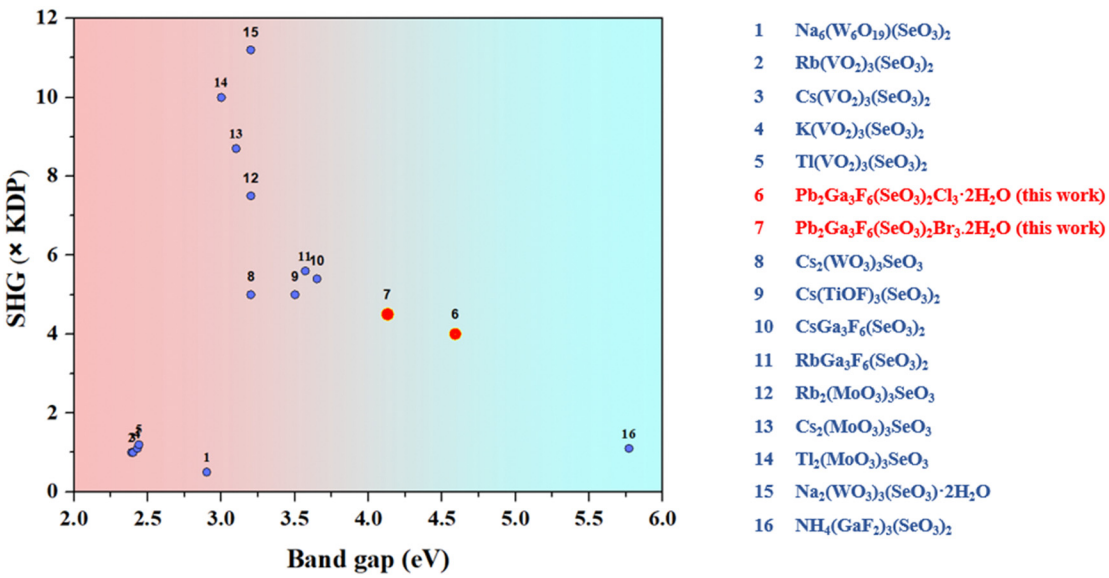

Fig. 6 The band gaps and SHG effects of current HTO-type NLO selenites.

Published on 05 March 2024. Downloaded by University of Houston on 12/13/2024 5:21:31 PM.

this family. On the structural aspect, $Pb_2Ga_3F_6(SeO_3)_2X_3{\cdot}2H_2O$ feature the typical HTO-type $[Ga_3F_6(SeO_3)_2]_\infty$ layer. The two compounds have relatively larger band gaps in the current NLO HTO family, and the values are 4.59 and 4.13 eV, respectively. Besides, they still exhibit strong SHG effects 4.0 and 4.5 times of KDP. Therefore, the title compounds $Pb_2Ga_3F_6(SeO_3)_2X_3{\cdot}2H_2O$ achieve a good balance between wide band gaps and large SHG effects. However, they cannot meet the type-I phase matchable conditions due to their small birefringences. The successful findings of $Pb_2Ga_3F_6(SeO_3)_2X_3{\cdot}2H_2O$ compounds not only enrich the HTO family, but also verify that it is effective to design new NLO crystals using the anion-mixing and cation group substitution strategies.

Author contributions

Lili Liu: supervision and writing – original draft. Junbo Wang: investigation. Bingchen Xiao: investigation. Yaoqing Chu: writing – review and editing. Xunchi Li: writing – review and editing. Tongqing Sun: writing – review and editing. P. Shiv Halasyamani: writing – review and editing.

Conflicts of interest

There are no conflicts to declare.

Acknowledgements

This work was supported by the Shanghai Institute of Technology (10120K238005-A06), the Welch Foundation (Grant E-1457), and the NSF (DMR-2002319).

Notes and references

1 W. Yao, R. He, X. Wang, Z. Lin and C. Chen, Analysis of Deep-UV Nonlinear Optical Borates: Approaching the End, *Adv. Opt. Mater.*, 2014, **2**, 411–417.

2 Z. Lin, W. Chen, Q. Lou, W. Fan, S. Xiang and H. Xue, Review on the Recent Progress of Laser Frontiers in China, *Sci. China: Technol. Sci.*, 2013, **56**, 1571–1588.

3 T. T. Tran, H. Yu, J. M. Rondinelli, K. R. Poeppelmeier and P. S. Halasyamani, Deep Ultraviolet Non-linear Optical Materials, *Chem. Mater.*, 2016, **28**, 5238–5258.

4 H. Sha, Z. Xiong, J. Xu, Z. Wang, R. Su, C. He, X. Yang, X. Long and Y. Liu, Phosphogermanate Crystal: A New Ultraviolet-Infrared Nonlinear Optical Crystal with Excellent Optical Performances, *ACS Appl. Mater. Interfaces*, 2022, **14**, 10588–10593.

5 X. Zhang, L. Kang, P. Gong, Z. Lin and Y. Wu, Nonlinear Optical Oxythiophosphate Approaching the Good Balance with Wide Ultraviolet Transparency, Strong Second Harmonic Effect, and Large Birefringence, *Angew. Chem., Int. Ed.*, 2020, **60**, 6386–6390.

6 W. Zeng, X. Dong, Y. Tian, L. Huang, H. Zeng, Z. Lin and G. Zou, Unprecedented Boat-Shaped $[Mo_2O_5(IO_3)_4]^{2-}$ Polyanions Induced a Strong Second Harmonic Generation Response, *Chem. Commun.*, 2022, **58**, 3350–3353.

7 E. E. Oyeka, M. J. Winiarski, H. Swiatek, W. Balliew, C. D. McMillen, M. Liang, M. Sorolla, II and T. T. Tran, $Ln_2(SeO_3)_2(SO_4)(H_2O)_2$ (Ln = Sm, Dy, Yb): A Mixed-Ligand Pathway to New Lanthanide (III) Multifunctional Materials Featuring Nonlinear Optical and Magnetic Anisotropy Properties, *Angew. Chem., Int. Ed.*, 2022, **61**, e202213499.

8 F. Kong and J. Mao, Recent Progress in Selenite and Tellurite Based SHG Materials, *Dalton Trans.*, 2020, **49**, 8433–8437.

9 J. Zhou, P. Xie, C. Wang, T. Bian, J. Chen, Y. Liu, Z. Guo, C. Chen, X. Pan, M. Luo, J. Yin and L. Mao, Hybrid Double Perovskite Derived Halides Based on Bi and Alkali Metals (K, Rb): Diverse Structures, Tunable Optical Properties and Second Harmonic Generation Responses, *Angew. Chem., Int. Ed.*, 2023, e202307646.

10 Y. Yang, Y. Xiao, B. Li, Y. Chen, P. Guo, B. Zhang and X. Zhang, Stereochemically Active Lone-Pair Containing Metal Substitution in Polar Axis toward a Giant Phase-Matchable Optical Nonlinear Silicate Crystal $Li_3(OH)PbSiO_4$, *J. Am. Chem. Soc.*, 2023, **145**, 22577–22583.

11 N. Ma, J. Chen, B. Li, C. Hu and J. Mao, $(NH_4)_2(I_5O_{12})(IO_3)$ and $K_{1.03}NH_{40.97}(I_5O_{12})(IO_3)$: Mixed-Valent Polyiodates with Unprecedented I_5O_{12}- Unit Exhibiting Strong Second-Harmonic Generation Responses and Giant Birefringence, *Small*, 2023, e2304388.

12 X. Lu, Z. Chen, X. Shi, Q. Jing and M. H. Lee, Two Pyrophosphates with Large Birefringences and Second-Harmonic Responses as Ultraviolet Nonlinear Optical Materials, *Angew. Chem., Int. Ed.*, 2020, **59**, 17648–17656.

13 L. Lin, X. Jiang, C. Wu, L. Li, Z. Lin, Z. Huang, M. G. Humphrey and C. Zhang, $Ba(MoO_2F)_2(XO_3)_2$ (X = Se and Te): First Cases of Noncentrosymmetric Fluorinated Molybdenum Oxide Selenite/Tellurite Through Unary Substitution for Enlarging Band Gaps and Second Harmonic Generation, *ACS Appl. Mater. Interfaces*, 2020, **12**, 49812–49821.

14 K. M. Ok, Toward the Rational Design of Novel Noncentrosymmetric Materials: Factors Influencing the Framework Structures, *Acc. Chem. Res.*, 2016, **49**, 2774–2785.

15 L. Liu, J. Young, M. Smeu and P. S. Halasyamani, $Ba_4B_8TeO_{19}$: A UV Nonlinear Optical Material, *Inorg. Chem.*, 2018, **57**, 4771–4776.

16 Y. Lan, J. Ren, P. Zhang, X. Dong, L. Huang, L. Cao, D. Gao and G. Zou, $ASb(SO_4)_2$ (A = Rb, Cs): Two short-wave UV antimony sulfates exhibiting large birefringence, *Chin. Chem. Lett.*, 2024, **35**, 108652.

17 X. Wang, X. Leng, Y. Kuk, J. Lee, Q. Jing and K. M. Ok, Deep-Ultraviolet Transparent Mixed Metal Sulfamates with Enhanced Nonlinear Optical Properties and Birefringence, *Angew. Chem., Int. Ed.*, 2023, e202315434.

18 Y. Xu, C. Lin, D. Zhao, B. Li, L. Cao, N. Ye and M. Luo, Chemical Substitution - Oriented Design of a New Polar $PbFIO_3$ Achieving a Balance Between Large Second-Harmonic Generation Response and Wide Band Gap, *Scr. Mater.*, 2022, **208**, 114347.

 This journal is © The Royal Society of Chemistry 2024

Published on 05 March 2024. Downloaded by University of Houston on 12/13/2024 5:21:31 PM.

19 R. Wang, F. Liang, X. Liu, Y. Xiao, Q. Liu, X. Zhang, L. M. Wu, L. Chen and F. Huang, Heteroanionic Melilite Oxysulfide: A Promising Infrared Nonlinear Optical Candidate with a Strong Second-Harmonic Generation Response, Sufficient Birefringence, and Wide Bandgap, *ACS Appl. Mater. Interfaces*, 2022, **14**, 23645–23652.

20 Y. Yang, X. Liu, J. Lu, L. Wu and L. Chen, $[Ag(NH_3)_2]_2SO_4$: A Strategy for the Coordination of Cationic Moieties to Design Nonlinear Optical Materials, *Angew. Chem., Int. Ed.*, 2021, **60**, 21216–21220.

21 G. Zou and K. M. Ok, Novel Ultraviolet (UV) Nonlinear Optical (NLO) Materials Discovered by Chemical Substitution-Oriented Design, *Chem. Sci.*, 2020, **11**, 5404–5409.

22 X. Chen and K. M. Ok, Metal Oxyhalides: An Emerging Family of Nonlinear Optical Materials, *Chem. Sci.*, 2022, **13**, 3942–3956.

23 J. Wang, M. Zhu, Y. Chu, J. Tian, L. Liu, B. Zhang and P. S. Halasyamani, Rational Design of the Alkali Metal Sn-Based Mixed Halides with Large Birefringence and Wide Transparent Range, *Small*, 2023, e2308884.

24 J. Chen, C. Hu, X. Zhang, B. Li, B. Yang and J. Mao, $CsVO_2F(IO_3)$: An Excellent SHG Material Featuring an Unprecedented 3D $[VO_2F(IO_3)]^-$ Anionic Framework, *Angew. Chem., Int. Ed.*, 2020, **59**, 5381–5384.

25 G. Zou, H. Jo, S. J. Lim, T. S. You and K. M. Ok, $Rb_3VO(O_2)_2CO_3$: A Four-in-One Carbonatoperoxovanadate Exhibiting an Extremely Strong Second-Harmonic Generation Response, *Angew. Chem., Int. Ed.*, 2018, **57**, 8619–8622.

26 L. Liu, B. Zhang, P. S. Halasyamani and W. Zhang, $Pb_2TiFO(SeO_3)_2Br$: A New Polar Compound with the Strongest Second Harmonic Generation in the Selenite Bromide Family, *J. Mater. Chem. C*, 2021, **9**, 6491–6497.

27 T. Wu, X. Jiang, C. Wu, Y. Hu, Z. Lin, Z. Huang, M. G. Humphrey and C. Zhang, Ultrawide Bandgap and Outstanding Second-Harmonic Generation Response by a Fluorine-Enrichment Strategy at a Transition-Metal Oxyfluoride Nonlinear Optical Material, *Angew. Chem., Int. Ed.*, 2022, **61**, e202203104.

28 X. Shi, A. Tudi, M. Cheng, F. Zhang, Z. Yang, S. Han and S. Pan, Noncentrosymmetric Rare-Earth Borate Fluoride $La_2B_5O_9F_3$: A New Ultraviolet Nonlinear Optical Crystal with Enhanced Linear and Nonlinear Performance, *ACS Appl. Mater. Interfaces*, 2022, **14**, 18704–18712.

29 Y. Li, W. Huang, Y. Zhou, X. Song, J. Zheng, H. Wang, Y. Song, M. Li, J. Luo and S. Zhao, A High-Performance Nonlinear Optical Crystal with a Building Block Containing Expanded pi-Delocalization, *Angew. Chem., Int. Ed.*, 2023, **62**, e202215145.

30 C. Jiang, X. Jiang, C. Wu, Z. Huang, Z. Lin, M. G. Humphrey and C. Zhang, Isoreticular Design of $KTiOPO_4$-Like Deep-Ultraviolet Transparent Materials Exhibiting Strong Second-Harmonic Generation, *J. Am. Chem. Soc.*, 2022, **144**, 20394–20399.

31 C. Wu, T. Wu, X. Jiang, Z. Wang, H. Sha, L. Lin, Z. Lin, Z. Huang, X. Long, M. G. Humphrey and C. Zhang, Large Second-Harmonic Response and Giant Birefringence of $CeF_2(SO_4)$ Induced by Highly Polarizable Polyhedra, *J. Am. Chem. Soc.*, 2021, **143**, 4138–4142.

32 G. Shi, Y. Wang, F. Zhang, B. Zhang, Z. Yang, X. Hou, S. Pan and K. R. Poeppelmeier, Finding the Next Deep-Ultraviolet Nonlinear Optical Material: $NH_4B_4O_6F$, *J. Am. Chem. Soc.*, 2017, **139**, 10645–10648.

33 X. Wang, Y. Wang, B. Zhang, F. Zhang, Z. Yang and S. Pan, CsB_4O_6F: A Congruent-Melting Deep-Ultraviolet Nonlinear Optical Material with Superior Functional Units Recombination, *Angew. Chem., Int. Ed.*, 2017, **56**, 14119–14123.

34 Y. Hu, X. Jiang, T. Wu, Y. Xue, C. Wu, Z. Huang, Z. Lin, J. Xu, M. G. Humphrey and C. Zhang, Wide Bandgaps and Strong SHG Responses of Hetero-Oxyfluorides by Dual-Fluorination-Directed Bandgap Engineering, *Chem. Sci.*, 2022, **13**, 10260–10266.

35 F. Kong, T. Jiang and J. Mao, Role of Fluorine on the Structure and Second-Harmonic-Generation Property of Inorganic Selenites and Tellurites, *Chem. Commun.*, 2021, **57**, 12575–12586.

36 Q. Huang, C. Hu, B. Yang, Z. Fang, Y. Lin, J. Chen, B. Li and J. Mao, $[GaF(H_2O)][IO_3F]$: a promising NLO material obtained by anisotropic polycation substitution, *Chem. Sci.*, 2021, **12**, 9333–9338.

37 C. Wu, X. Jiang, L. Lin, Z. Lin, Z. Huang, M. G. Humphrey and C. Zhang, $AGa_3F_6(SeO_3)_2$ (A = Rb, Cs): A New Type of Phase-Matchable Hexagonal Tungsten Oxide Material with Strong Second-Harmonic Generation Responses, *Chem. Mater.*, 2020, **32**, 6906–6915.

38 X. Cao, C. Hu, F. Kong and J. Mao, $Cs(TaO_2)_3(SeO_3)_2$ and $Cs(TiOF)_3(SeO_3)_2$: structural and second harmonic generation changes induced by the different d^0-TM coordination octahedra, *Inorg. Chem.*, 2015, **54**, 3875–3882.

39 H. Y. Chang, S. W. Kim and P. S. Halasyamani, Polar Hexagonal Tungsten Oxide (HTO) Materials: (1) Synthesis, Characterization, Functional Properties, and Structure−Property Relationships in $A_2(MoO_3)_3(SeO_3)$ (A = Rb+ and T^I+) and (2) Classification, Structural Distortions, and Second-Harmonic Generating Properties of Known Polar HTOs, *Chem. Mater.*, 2010, **22**, 3241–3250.

40 S. D. Nguyen and P. S. Halasyamani, Synthesis, structure, and characterization of two new polar sodium tungsten selenites: $Na_2(WO_3)_3(SeO_3).2H_2O$ and $Na_6(W_6O_{19})(SeO_3)_2$, *Inorg. Chem.*, 2013, **52**, 2637–2647.

41 G. Park and K. M. Ok, Hexagonal Tungsten Oxides with Large Bandgaps Synthesized by a Chemical Substitution Method, *Inorg. Chem. Front.*, 2020, **7**, 4469–4476.

42 SAINT, *version 7.60A Bruker Analytical X-ray Instruments*, Inc.: Madison, WI, 2008.

43 G. M. Sheldrick, *SHELXTL, version 6.14; Bruker Analytical Xray Instruments*, Inc.: Madison, WI, 2003.

44 G. M. Sheldrick, Crystal Structure Refinement with SHELXL, *Acta Cryst.*, 2015, **C71**, 3–8.

45 A. L. Spek, Single-Crystal Structure Validation with the Program PLATON, *J. Appl. Cryst.*, 2003, **36**, 7–13.

46 N. E. Brese and M. Okeeffe, Bond-Valence Parameters for Solids, *Acta Cryst.*, 1991, **B47**, 192–197.

Published on 05 March 2024. Downloaded by University of Houston on 12/13/2024 5:21:31 PM.

47 S. K. Kurtz and T. T. Perry, A Powder Technique for Evaluation of Nonlinear Optical Materials, *J. Appl. Phys.*, 1968, **39**, 3798–3813.
48 S. J. Clark, M. D. Segall, C. J. Pickard, P. J. Hasnip, M. J. Probert, K. Refson and M. C. Payne, First Principles Methods Using CASTEP, *Z. Kristallogr.*, 2005, **220**, 567–570.
49 J. P. Perdew, K. Burke and M. Ernzerhof, Generalized Gradient Approximation Made Simple, *Phys. Rev. Lett.*, 1996, **77**, 3865–3868.
50 A. M. Rappe, K. M. Rabe, E. Kaxiras and J. D. Joannopoulos, Optimized Pseudopotentials, *Phys. Rev. B: Condens. Matter Mater. Phys.*, 1990, **41**, 1227–1230.
51 G. S. Xiong, G. X. Lan, H. F. Wang and C. O. Huang, Infrared Reflectance And Raman-Spectra Of Lithium Triborate Single-Crystal, *J. Raman Spectrosc.*, 1993, **24**, 785–789.
52 S. Yan, X. Wang, C. Hu, B. Li, F. Kong and J. Mao, $Na_3Ti_3O_3(SeO_3)_4F$: A Phase-Matchable Nonlinear-Optical Crystal with Enlarged Second-Harmonic-Generation Intensity and Band Gap, *Inorg. Chem.*, 2022, **61**, 2686–2694.
53 F. You, F. Liang, Q. Huang, Z. Hu, Y. Wu and Z. Lin, $Pb_2GaF_2(SeO_3)_2Cl$: Band Engineering Strategy by Aliovalent Substitution for Enlarging Bandgap while Keeping Strong Second Harmonic Generation Response, *J. Am. Chem. Soc.*, 2019, **141**, 748–752.
54 S. Shi, C. Lin, D. Zhao, M. Luo, L. Cao, G. Peng and N. Ye, Unexpected Aliovalent Cation Substitution Between Two NLO Materials $LiBa_3Bi_6(SeO_3)_7F_{11}$ and $Ba_3Bi_{6.5}(SeO_3)_7F_{10.5}O_{0.5}$, *Chem. Commun.*, 2021, **57**, 2982–2985.
55 S. Shi, C. Lin, G. Yang, L. Cao, B. Li, T. Yan, M. Luo and N. Ye, $A_2Bi_2(SeO_3)_3F_2$ (A = K and Rb): Excellent Mid-Infrared Nonlinear Optical Materials with Both Strong SHG Responses and Large Band Gaps, *Chem. Mater.*, 2020, **32**, 7958–7964.
56 C. Liu, S. Zhou, Y. Xiao, C. Zhang, H. Lin and Y. Liu, Aliovalent-Cation-Substitution-Induced Structure Transformation: A New Path Toward High-Performance IR Nonlinear Optical Materials, *J. Mater. Chem. C*, 2021, **9**, 15407–15414.
57 C. Liu, S. Zhou, Y. Xiao, C. Zhang, Y. Shen, X. Liu, H. Lin and Y. Liu, $CsCu_3SbS_4$: Rational Design of a Two-Dimensional Layered Material with Giant Birefringence Derived from Cu_3SbS_4, *Inorg. Chem. Front.*, 2022, **9**, 478–484.
58 X. Chen, S. Zhou, C. Zhang, H. Lin and Y. Liu, A Novel Bifunctional Thioarsenate Based on Unprecedented Molecular $[Cd_4As_8Se_{16}(Se_2)_2]^{8-}$ Cluster Anions, *Chem. Commun.*, 2023, **59**, 12124–12127.
59 C. Zhang, M. Ran, X. Chen, S. Zhou, H. Lin and Y. Liu, Stereochemically Active Lone-Pair-Driven Giant Enhancement of Birefringence from Threedimensional $CsZn_4Ga_5Se_{12}$ to Two-Dimensional $CsZnAsSe_3$, *Inorg. Chem. Front.*, 2023, **10**, 3367–3374.

 This journal is © The Royal Society of Chemistry 2024